An analytical model to study the dynamic response of heat exchanger network

Rupu Yang, Cong Toan Tran, Zoughaib Assaad

An analytical model to study the dynamic response of heat exchanger network

Rupu YANG[a], Cong Toan Tran[b*], Assaad Zoughaib[b]

a *Policy Research Center for Environment and Economy, Ministry of Ecology and Environment of the PR China, 100029 Beijing , China*

b *MINES ParisTech, PSL Research University, CES (Center for Energy efficiency of Systems), 5, rue Léon Blum, 91120 Palaiseau, France*

Abstract: An analytical model for the heat exchanger network (HEN) has been proposed in this work to study the dynamic performance of HEN in the design stage. The model relies on the Laplace transform to obtain the system outlet temperature function when facing operational changeover. Equipped with the decomposition strategy and pathway analysis, the model can reach the system outlet temperature function in the time domain in an easy way and free of the numerical difficulty concern caused by the inverse Laplace transform process that may occur toward complicated expressions. The potential bias of the model has been illustrated both in static and dynamic aspects by changing the operational conditions of a heat exchanger. The analytical model has been applied in a four streams HEN synthesis problem to investigate the trade-off result between the economic cost and the response time. Moreover, the comparison with the simulation result toward selected HENs has shown that the proposed model may act as a pre-selection tool to predict the dynamic performance of various HENs during the design stage.

Key words: heat exchanger network, analytical model, response time, dynamic performance, synthesis

Nomenclature

a	Variable in the analytical model
A	Heat transfer area, m^2
AMTD	Arithmetic mean temperature difference
b	Variable in the analytical model
CCU	Cost of cold utility, \$/(kW•yr)
CHU	Cost of hot utility, \$/(kW•yr)
CP	Specific heat capacity of stream, J/K
CU	Cold utility
f	Variable in the heat exchanger dynamic model
g	Variable in the heat exchanger dynamic model
G	Function of the specific pathway in Laplace domain
h	Heat transfer coefficient, (kW/m^2•K)
hcu	Heat transfer coefficient of cold utility, (kW/m^2•K)
hhu	Heat transfer coefficient of hot utility, (kW/m^2•K)
HE	Heat exchanger
HEN	Heat exchanger network
HU	Hot utility
M	Mass of metal wall
r	Variable in the heat exchanger dynamic model
s	Laplace variable

SA	Simulated annealing
t	Time variable, s
T	Stream temperature, K
TAC	Total annual cost
x	Variable in the heat exchanger dynamic model
z	Variable in the heat exchanger dynamic model
λ	Bypass ratio

Subscripts and superscripts

c	Cold side
cu	Cold utility
h	Hot side
hu	Hot utility
in	Inlet
o	Outlet
wall	Metal wall of heat exchanger

1. Introduction

Heat exchanger network (HEN) applied widely in the industrial system to reduce the energy and utility consumption. The HEN describes a network composed of a number of heat exchangers (HEs) that connect various hot and cold streams. The HEN design has started from last 70s, it usually aims to reduce the energy consumption from utilities and also optimize the system cost. Considerable efforts have been devoted to improve the HEN design method and to consider the operability issues such as the flexibility and controllability. The importance of the HEN response time has already been recognized in the literatures. Picon-Nunez and Polley [1] introduced the need to consider the impact of changes in heat transfer performance in networks. Liu et al. [2] mentioned that the time response in the evolution of flexibility study has to be settled. Jogwar et al. [3]argued the importance to enable the HEN achieve fast transient. The previous work in our group [4] showed that the economic optimal heat integrated system illustrates evident long transition time when change the load of the HEN from the nominal one to 50% of load, since the design relies on the Pinch technology that can only consider static performance. In one of the latest thesis in the domain of HEN design [5], the author studied a real case problem where the system ran in 2 operating conditions and the transition duration between them could be about 2.5 hours to 3.5 hours, corresponding roughly to 30% of the working period. Knowing that during the transition phase the system's products may miss the required specifications, it might represent a loss for the production. Thus, it is crucial to explore the response time performance when there is an operational changeover of HEN in the design stage, to guarantee an excellent dynamic performance, and there is urgent requirement to find efficient method to study the HEN dynamic performance. It should be noted that most of the available HEN design methods are based on the static indicators to deal with the HEN dynamic performance, and they require validations with dynamic studies [6][7][8].

There are many efforts devoted to exploring HEN dynamic performance. In general, it can be classified in two ways: numerical simulation or analytical models. In the simulation approach, the objective is to use available numerical methods or simulation tools to solve the governing equations of the problem (mass and energy

balances), while in the analytical approach the different variables of a HEN can be expressed by a function of the known parameters (such as heat transfer areas…) and the inlet information of the HEN (inlet flowrates and temperatures). The hybrid methods to combine the numerical simulation and analytical model might also be a solution, which has been applied in single HE design [9][10][11], but the application in the dynamic performance study of HEN has rarely been discussed.

Papastratos et al. [12] followed the simulation approach by utilizing the SpeedUp dynamic process simulator. Mathisen and Morari [13] proposed a HEN dynamic model based on the lumped model for single HE, with the main focus on the discussion about the model features for HE and HEN. As for the dynamic performance, their target is to avoid the control difficulty caused by the inverse response, and the dynamic result is obtained through MATLAB/Simulink. In their model, the number of cells describing the HE dynamic model determines the accuracy, and they provided a range to select this number. Their approach does not fit complex HEN structures because of the complexity, computational speed, and numerical stability, as argued by Chen et al. [14]. Boyaci et al. [15] constructed a HEN dynamic model based on a distributed-parameter model of multi-tubes, single-pass for HEs. They mainly focused on comparing HEN dynamic response under the scenarios of open-loop bypass control and closed-loop bypass control, and they employed the LSODES to solve their dynamic models. Similar researches to study HEN dynamic response under the effect of bypasses through the simulation are reported in [16][17].

Until recently, Chen et al. [14] provided an analytic method to study the transient behavior of HEN facing disturbances, which can be a promising method to achieve better control performance of HEN. In their work, the HE model was described with a first-order model, and the model enables engineers to obtain transfer function between any two nodes of HEN, which is a relatively convenient method to study HEN dynamic behavior. Nevertheless, their method aims to predict the system transient behavior facing quite small disturbances, which is not suitable for studying the operational change case.

Table 1 summarizes the comparison between the numerical simulation and analytical ways to reach the HEN dynamic performance. The numerical simulation approach can function well for most HEN conditions, it can also be a fast solution when calculating a specific HEN inlet changeover condition. However, the application of simulation in a HEN design problem might not be suitable considering the potential enormous testing cases and the corresponding high computational cost. Comparatively, the analytical method might be a more promising way to study the dynamic performance of the HEN in the design problem. Developing an analytical solution may take time, but the computational cost to get the numerical results is expected to be much lower than the simulation approach when the analytical solution is known. Therefore, the study of HEN dynamic performance problem is transferred to the construction of the HEN dynamic model to obtain the outlet temperature function when there is an operational changeover.

The current available analytical method is insufficient to undertake substantial inlet parameter change of a HEN. HE is the fundamental element of a HEN, the available analytical models of a single HE should be reviewed. Traditional analytical methods deal with Laplace transform over energy balance governing equations and end up with a rather complicated expression just for only one HE [18], and it can hardly be extended to obtain the

HEN outlet temperature. The main advantage of the traditional method is the capability to explore the temperature distribution inside the HE. Many authors adopted such a point to simplify the model by selecting the first-order model to approach the dynamic performance of the HE, and such choice originated from the observation of experimental results. But most studies only reported the single inlet parameter change condition [19][20][21], without discussing the possibility to explore the simultaneous change scenario. Yin and Jensen [22] suggested the integral approach which extends from the work by [23]. They assumed that the first-order model could describe transient temperature, and stable temperature decided by the NTU method, without showing the potential to handle simultaneous parameter change scenario. The analytic model suggested by [24] is able to deal with arbitrary temperature change, the mass flow rate dependent parameters conditions, and the temperature distributions. However, their lumped HE dynamic model requires experimental or numerical simulations results to calibrate the corresponding parameters, and that makes the model impossible to be used for a HEN design problem. Chen et al. [14] tried to study the simultaneous disturbance effect on outlet temperature by deriving potential gain and time constant toward various types of small disturbances based on the first-order transfer function originated from [25]. The developed model is inappropriate when the operational change of the network is significant.

The comparison of HE analytical methods to study the dynamic performance is provided in Table 2. The targeted HE analytic model is expected to deal with simultaneous changes that can be both small and significant and be appropriate for any form of change in HE inlet. Laplace transform might be the most suitable approach to construct the HE dynamic model in this context, and a simplified method can be explored by ignoring the temperature distribution inside the HE.

In what follows, a simplified HE dynamic model will be introduced at first, then the paper will provide a strategy to develop a HEN dynamic model that can help to study the response time when there is operational changeover. Finally, a case study will be employed to illustrate the application of the analytical model in the HEN synthesis.

2. Math models

2.1 HE dynamic model

The HE dynamic model is the basis to develop the HEN model. Several assumptions are made to simplify the HE model,

- When there is an inlet variation, stream mass flow rate changes instantly (in other words, the change is in the form of the step function), and there is no time delay from the inlet port to the outlet port of the network because the fluid is supposed to be incompressible.
- Stream heat transfer coefficients may be different according to the operational conditions, but during the transient phase they are supposed to keep constant and be equal to the values corresponding to the new operational condition.
- The temperature of the HE metal wall is uniform.

As depicted in Fig. 1, the HE is assumed to be in counter-current flow configuration, which is coherent with most actual industry cases. The energy balance equations can be formulated as in eqs. (1) to (3) where the indexes h, c, wall, in, and o stand for the hot stream, cold stream, HE metal wall, inlet, and outlet, respectively. M, c, CP, h and A stand for mass, heat capacity, heat capacity flow, heat transfer coefficient, and heat transfer area. It should be noted that the heat transfer is calculated via the arithmetic mean temperature difference (AMTD), which is an acceptable choice to simplify the model. Indeed, Girei [26] also adopted the AMTD to study the operating issues of HEN in his doctoral thesis. This model provides the exact solution when the HE size is small enough. For a large HE, the error caused by the average temperature assumption will be quantified in the next part.

$$CP_h\left(T_{h,in}(t)-T_{h,o}(t)\right)=A_h h_h\left(\left(T_{h,in}(t)+T_{h,o}(t)\right)/2-T_{wall}(t)\right) \quad (1)$$

$$CP_c\left(T_{c,o}(t)-T_{c,in}(t)\right)=A_c h_c\left(T_{wall}(t)-\left(T_{c,in}(t)+T_{c,o}(t)\right)/2\right) \quad (2)$$

$$CP_h\left(T_{h,in}(t)-T_{h,o}(t)\right)=CP_c\left(T_{c,o}(t)-T_{c,in}(t)\right)+M_{wall}c_{wall}\frac{dT_{wall}(t)}{dt} \quad (3)$$

Expressing $T_{h,o}(t)$ and $T_{c,o}(t)$ with $T_{wall}(t)$, $T_{h,in}(t)$ and $T_{c,in}(t)$ by reformulating eq. (1) and eq. (2) :

$$T_{c,o}(t)=\left(h_c A_c T_{wall}(t)+\left(CP_c-h_c A_c/2\right)T_{c,in}(t)\right)/\left(CP_c+h_c A_c/2\right) \quad (4)$$

$$T_{h,o}(t)=\left(h_h A_h T_{wall}(t)+\left(CP_h-h_h A_h/2\right)T_{h,in}(t)\right)/\left(CP_h+h_h A_h/2\right) \quad (5)$$

Taking eq. (4) and eq. (5) into eq. (3) by seeking the relationship between $T_{wall}(t)$, $T_{h,in}(t)$ and $T_{c,in}(t)$, eq. (6) can be reached:

$$M_{wall}c_{wall}\frac{dT_{wall}(t)}{dt}+\frac{CP_h h_h A_h}{CP_h+\frac{h_h A_h}{2}}T_{wall}(t)+\frac{CP_c h_c A_c}{CP_c+\frac{h_c A_c}{2}}T_{wall}(t)=\frac{CP_h h_h A_h}{CP_h+\frac{h_h A_h}{2}}T_{h,in}(t)+\frac{CP_c h_c A_c}{CP_c+\frac{h_c A_c}{2}}T_{c,in}(t) \quad (6)$$

The HE is expected to operate under various operational periods, heat capacity flow and inlet temperature will change at the period change time. Considering the time after the period change, while the temperatures vary with time, the heat capacity flow rates can be regarded as constant because their variations follow the step functions. Taking Laplace transform over eq. (6) just after the operation period change from period 1 to period 2, the temperature of the metal wall in Laplace domain can be expressed as following:

$$T_{wall}(s)=\frac{r_h T_{h,in}(s)+r_c T_{c,in}(s)+M_{wall}c_{wall}T_{wall}(0)}{M_{wall}c_{wall}s+r_h+r_c},\ where\ r_h=\frac{CP_h h_h A_h}{CP_h+\frac{h_h A_h}{2}}, r_c=\frac{CP_c h_c A_c}{CP_c+\frac{h_c A_c}{2}} \quad (7)$$

All the parameters correspond to period 2. $T_{wall}(0)$ is the wall temperature at the time 0, and it is determined by the heat transfer coefficients together with the stream temperatures before the operation period change (i.e. in the period 1, *p1*), and described as:

$$T_{wall}(0)=\left.\frac{h_h A_h(T_{h,in}(0)+T_{h,o}(0))+h_c A_c(T_{c,in}(0)+T_{c,o}(0))}{2(h_h A_h+h_c A_c)}\right|_{p1} \quad (8)$$

Taking Laplace transform over eqs. (4) and (5):

$$T_{c,o}(s)=x_c T_{wall}(s)+z_c T_{c,in}(s) \quad (9)$$

$$T_{h,o}(s)=x_h T_{wall}(s)+z_h T_{h,in}(s) \quad (10)$$

where, $x_h=\frac{h_h A_h}{CP_h+\frac{h_h A_h}{2}}$, $x_c=\frac{h_c A_c}{CP_c+\frac{h_c A_c}{2}}$, $z_c=\frac{CP_c-\frac{h_c\times A_c}{2}}{CP_c+\frac{h_c\times A_c}{2}}$ and $z_h=\frac{CP_h-\frac{h_h A_h}{2}}{CP_h+\frac{h_h A_h}{2}}$.

Finally taking (7) to (9) and (10), the outlet temperatures of the cold and hot streams can be obtained in Laplace form:

$$T_{h,o}(s)=f_{11}\cdot T_{h,in}(s)+f_{12}\cdot T_{h,in}(s)+f_2\cdot T_{c,in}(s)+f_3\cdot T_{wall}(0) \tag{11}$$

$$T_{c,o}(s)=g_{11}\cdot T_{c,in}(s)+g_{12}\cdot T_{c,in}(s)+g_2\cdot T_{h,in}(s)+g_3\cdot T_{wall}(0) \tag{12}$$

Where coefficient functions f and g are functions in Laplace domain that are detailed in eqs. (13) to (20). The outlet temperature function is composed of four parts where the coefficient functions are all in the form of $\frac{b}{s+a}$ or $const$ (where a, b and const are known parameters). Such formulation aims to decompose the outlet temperature function into small parts of which the coefficients can share the same form that facilitates further analysis in the HEN level. It can also be interpreted that there are four pathways from the inlet source to the outlet target in a HE, the coefficient function corresponds to the transfer function of each pathway as shown in Fig. 2 for the outlet temperature of a HE, and the outlet temperature function equals to the sum of the effects of all pathways.

$$f_{11}=\frac{CP_h\cdot h_h\cdot A_h}{CP_h+h_h\cdot A_h/2}\cdot\frac{h_h\cdot A_h}{CP_h+h_h\cdot A_h/2}\Bigg/\left(M_{wall}c_{wall}\cdot s+\frac{CP_h\cdot h_h\cdot A_h}{CP_h+h_h\cdot A_h/2}+\frac{CP_c\cdot h_c\cdot A_c}{CP_c+h_c\cdot A_c/2}\right) \tag{13}$$

$$f_{12}=\left(CP_h-h_h\cdot A_h/2\right)\Big/\left(CP_h+h_h\cdot A_h/2\right) \tag{14}$$

$$f_2=\left(\frac{CP_c\cdot h_c\cdot A_c}{CP_c+h_c\cdot A_c/2}\cdot\frac{h_h\cdot A_h}{CP_h+h_h\cdot A_h/2}\right)\Bigg/\left(M_{wall}c_{wall}\cdot s+\frac{CP_h\cdot h_h\cdot A_h}{CP_h+h_h\cdot A_h/2}+\frac{CP_c\cdot h_c\cdot A_c}{CP_c+h_c\cdot A_c/2}\right) \tag{15}$$

$$f_3=M_{wall}c_{wall}\cdot\frac{h_h\cdot A_h}{CP_h+h_h\cdot A_h/2}\Bigg/\left(M_{wall}c_{wall}\cdot s+\frac{CP_h\cdot h_h\cdot A_h}{CP_h+h_h\cdot A_h/2}+\frac{CP_c\cdot h_c\cdot A_c}{CP_c+h_c\cdot A_c/2}\right) \tag{16}$$

$$g_{11}=\frac{CP_c\cdot h_c\cdot A_c}{CP_c+h_c\cdot A_c/2}\cdot\frac{h_c\cdot A_c}{CP_c+h_c\cdot A_c/2}\Bigg/\left(M_{wall}c_{wall}\cdot s+\frac{CP_h\cdot h_h\cdot A_h}{CP_h+h_h\cdot A_h/2}+\frac{CP_c\cdot h_c\cdot A_c}{CP_c+h_c\cdot A_c/2}\right) \tag{17}$$

$$g_{12}=\left(CP_c-h_c\cdot A_c/2\right)\Big/\left(CP_c+h_c\cdot A_c/2\right) \tag{18}$$

$$g_2=\frac{CP_h\cdot h_h\cdot A_h}{CP_h+h_h\cdot A_h/2}\cdot\frac{h_c\cdot A_c}{CP_c+h_c\cdot A_c/2}\Bigg/\left(M_{wall}c_{wall}\cdot s+\frac{CP_h\cdot h_h\cdot A_h}{CP_h+h_h\cdot A_h/2}+\frac{CP_c\cdot h_c\cdot A_c}{CP_c+h_c\cdot A_c/2}\right) \tag{19}$$

$$g_3=M_{wall}c_{wall}\cdot\frac{h_c\cdot A_c}{CP_c+h_c\cdot A_c/2}\Bigg/\left(M_{wall}c_{wall}\cdot s+\frac{CP_h\cdot h_h\cdot A_h}{CP_h+h_h\cdot A_h/2}+\frac{CP_c\cdot h_c\cdot A_c}{CP_c+h_c\cdot A_c/2}\right) \tag{20}$$

2.2 HEN dynamic model

The pathway analysis of the whole network allows to construct the function of HEN outlet temperature. Two processes that connect various HEs in a HEN are required to be considered, which are HEs in series and stream split. In the following analysis, the HEN with a loop is out of the discussion. In what follows, two examples have been employed to illustrate the method.

In the first example, the condition when two HEs are in series has been studied, as shown in Fig. 3 (one hot stream H1 and two cold streams C1 and C2), in which the H1 outlet temperature is the target variable to be calculated. H1 transfers heat with C1 in HE E1 to reach $T_{h1,2}(s)$ at first, and then transfers heat with C2 in E2 to reach the outlet temperature $T_{h1,out}(s)$. As explained before, every outlet temperature of a given HE comprises four pathways from the inlet sources to the outlet target, and because the network is composed of 2 HEs in-series, there are two "steps" to reach $T_{h1,out}(s)$ from the inlet sources. The pathway analysis of this example is provided in Fig. 4. There are total 10 pathways and the corresponding transfer functions are listed in

Table 3. The transfer function of each pathway is obtained through the multiplication of each involved sub-functions. Then, $T_{h1,out}(s)$ is equal to the sum of all these transfer functions. Note that, the pathways function from the inlet to the outlet can be obtained directly without the necessity to calculate the intermediate temperature $T_{h1,2}(s)$.

The stream split enlarges the number of pathways and gives specific split ratios to the corresponding downstream paths. Here, another example (Fig. 5) is used to illustrate how to handle both HEs in-series and split-mixing process. It is a four-stream problem (two hot streams and two cold streams), and the outlet temperature of C2 is the target variable to be obtained. The pathway analysis diagram can be constructed, as shown in Fig. 6. It can be observed that there are five pathways to reach $T_{h2,2}$: four pathways coming from the HE E1, and the fifth one from the bypass. Calculating the transfer function of each pathway, the results are provided in Table A1.

There are 24 pathways from various sources to affect the outlet temperature of C2, and the target temperature function equals the sum of all these sub-functions. The next step is to carry out the inverse Laplace transform to obtain the temperature function in the time domain. Knowing that the inverse Laplace transform of a sum is equal to the sum of inverse Laplace transforms (eq. 21), the main question is how to carry out efficiently inverse Laplace transform of each sub-function.

$$\ell^{-1}\{F_1(s)+F_1(s)\}=\ell^{-1}\{F_1(s)\}+\ell^{-1}\{F_1(s)\} \tag{21}$$

Observing the sub-functions in Table A1, each of them is a product of the basic functions f and g, which are in the form of $\frac{b}{s+a}$ or $const$ (a, b and const are parameters depend on the specific HE and pathway). By applying the partial fraction decomposition, it is possible to decompose the sub-functions as a sum of simple fractions. The advantage of implementing such decomposition is that the simple fraction functions are standard expressions for which the inverse Laplace transform can be reached easily. To illustrate the method, the pathway 24 is selected as an example, and the inlet temperature $T_{hu,in}$ is assumed to follow step signal. Thus, the function of pathway 24 ($G_{24}(s)$) in Table A1 can be expressed as the eq. (22). $T_{hu,in}(0)$ is the temperature just before the step change which is a parameter, a and b are known and depend only on the parameters of the problem (their expressions can be obtained by comparing with the definition of the function g2, eq. 19). Eq. (22) can be decomposed into simple forms, as in the eq. (23), with the help of eq. (24). Finally, the function in the time domain can be reached as shown in eq. (25) by following the standard inverse Laplace transform table as reference. Since all the pathways' equations are similar to eq. (22), they can be decomposed into the simple forms as with eq. (23), and that allows to reach the corresponding functions in the time domain analytically. That is the reason to divide the outlet temperature function of HE in small parts, as shown in the eqs. (11) and (12), and propose to obtain the function by dealing with every pathway separately. The function in Laplace form and in the time domain of all the 24 pathways are provided in annex (Table A2) after applying the described decomposition method by assuming that all the inlet temperature changes in step forms. Note that the expressions of a and b depend on both the specific HE and the corresponding functions of f and g.

$$G_{24}(s)=\frac{T_{hu,in}(0)}{s}\cdot\frac{b_{g_2}^{HU}}{s+a^{HU}} \tag{22}$$

$$G_{24}(s)=\frac{T_{hu,in}(0)\cdot b_{g_2}^{HU}}{a^{HU}}\left(\frac{1}{s}-\frac{1}{s+a^{HU}}\right) \tag{23}$$

$$\frac{1}{s+a_1}\cdot\frac{1}{s+a_2}=\frac{1}{a_2-a_1}\left(\frac{1}{s+a_1}-\frac{1}{s+a_2}\right),a_2\neq a_1 \tag{24}$$

$$G_{24}(t)=\frac{T_{hu,in}(0)\cdot b_{g_2}^{HU}}{a^{HU}}\left(1-e^{-a^{HU}t}\right) \tag{25}$$

Another advantage of the above method is the capability to deal with the inlet temperature change in the other forms without limiting to the step signal, such as the ramp or the exponential signal. The pathway n° 24 is chosen as an example again to analyze various inlet temperature change forms. In the case where the inlet temperature follows a ramp function as in eq. (26), the corresponding function in the Laplace domain is shown in eq. (27). Thus, $G_{24}(s)$ can be reached as in eq. (28) and its function in the time domain is shown in eq. (29). When the inlet temperature changes with the exponential signal as shown in the eq. (30), the same method can be applied to obtain the temperature function in time domain directly from eq. (32) to eq. (33). Hence, the method can deal with any inlet change that can be represented as a combination of step, ramp, and exponential functions.

$$T_{hu,in}(t)=\begin{pmatrix} w+vt, 0\le t\le t_1; \\ w+vt_1, t>t_1 \end{pmatrix}, \text{ Ramp signal} \tag{26}$$

$$T_{hu,in}(s)=\begin{pmatrix} \frac{w}{s}+\frac{v}{s^2}, 0\le t\le t_1; \\ \frac{w+vt_1}{s}, t>t_1 \end{pmatrix} \tag{27}$$

$$G_{24}(s)=\begin{pmatrix} \left(\frac{w}{s}+\frac{v}{s^2}\right)\cdot\frac{b_{g_2}^{HU}}{s+a^{HU}}, 0\le t\le t_1; \\ \frac{w+vt_1}{s}\cdot\frac{b_{g_2}^{HU}}{s+a^{HU}}, t>t_1 \end{pmatrix} \tag{28}$$

$$G_{24}(t)=\begin{pmatrix} \frac{w\cdot b_{g_2}^{HU}}{a^{HU}}\cdot(1-e^{-a^{HU}t})+\frac{v\cdot b_{g_2}^{HU}}{(a^{HU})^2}\cdot(e^{-a^{HU}t}-1+a^{HU}t), 0\le t\le t_1; \\ \frac{(w+vt_1)\cdot b_{g_2}^{HU}}{a^{HU}}\cdot(1-e^{-a^{HU}t}), t>t_1 \end{pmatrix} \tag{29}$$

$T_{hu,in}(t)=w+ve^{ct}$, Exponential signal (30)

$$T_{hu,in}(s)=\frac{w}{s}+\frac{v}{s-c} \tag{31}$$

$$G_{24}(s)=\left(\frac{w}{s}+\frac{v}{s-c}\right)\cdot\frac{b_{g_2}^{HU}}{s+a^{HU}} \tag{32}$$

$$G_{24}(t)=\frac{w\cdot b_{g_2}^{HU}}{a^{HU}}\cdot(1-e^{-a^{HU}t})+\frac{v\cdot b_{g_2}^{HU}}{a^{HU}+c}\cdot(e^{-a^{HU}t}-e^{ct}) \tag{33}$$

In this section, a HEN model has been developed. The HEN outlet temperature function can be reached through the pathway analysis, in which the function of each corresponding pathway is the product of the simple form function. The core step is to carry out the partial fraction decomposition toward each pathway's function to transfer it into the sum of simple functions, and the inverse Laplace transform of those simple functions can be obtained directly from the standard Laplace transform table. Moreover, the methodology has been applied in various inlet temperature variation forms such as step signal, ramp signal, and exponential signal.

The identification of pathways requires two steps. The first one is to transfer the given HEN structure into a multi-directed graph, by setting HEs as nodes and mass/heat flows as directed edges. The second step is to apply the graph theory to find all the pathways for the given input and output nodes. In this paper, these two steps are done through the networkX package in Python. Then, the analytical model has been automated in Python to carry out the following case studies. The automated point is crucial in the context of a HEN design problem because there will be vast number of structures to be tested in a design problem, and manual calculation seems grossly inefficient.

3. Validation of the analytical model

As discussed above, the analytical model has been implemented in Python. The model is not a trivial one to implement and a quite long code has been required. Before applying such automated model in the forthcoming case problem, it is crucial to validate the implementation. After that, the potential bias of the model caused by the assumptions to simplify the analysis will be studied through a case problem. To do so, the comparison with finite volume method simulation results will be carried out.

3.1 Validation of the implementation of the analytical model

Here, Dymola is employed as the simulation tool to validate the implementation of the analytical model in Python. The HE model in Dymola follows the same governing equations as in eq. (1) – eq. (3). One of the optimized HENs presented in [27] is selected as an example to carry out the comparison study. It is a 10 streams case problem, as shown in Fig. 7 with HEN parameters listed in Table 4, and the outlet temperature of C1 is set as the target variable. The inlet temperatures are assumed to change in the form of step and ramp signal, and the inlet parameters are expected to change in three scenarios:

- scenario1 (S1): Inlet temperature change: the inlet temperatures of all hot streams increase 20 K, and the cold stream decrease 20 K.
- scenario2 (S2): Mass flow change: hot stream mass flows increase 10%, and cold stream decrease 10%.
- scenario3 (S3): Simultaneous temperature and mass flow change: The streams temperature and mass flow change simultaneously as the same value as in the above two scenarios.

Step signal

When the inlet parameters change with the step signal, the target temperature functions can be obtained by the above decomposition-based method and are provided as follows.

Scenario1 (S1) only inlet temperature change:

$$T_{c1,out}(t) = 438 - 119e^{(-0.049t)} + 40.4e^{(-0.060t)} + 1121e^{(-0.037t)} - 1122e^{(-0.036t)} + 80.8e^{(-0.031t)} \quad (34)$$

Scenario2 (S2) only inlet mass flowrate change:

$$T_{c1,out}(t) = 449 + 120e^{(-0.049t)} - 29.9e^{(-0.06t)} - 1130e^{(-0.037t)} + 1121e^{(-0.036t)} - 90.5e^{(-0.031t)} \quad (35)$$

Scenario3 (S3) simultaneous change:

$$T_{c1,out}(t) = 455 - 43.2e^{(-0.049t)} + 21.1e^{(-0.060t)} + 356e^{(-0.037t)} - 339e^{(-0.036t)} - 5.67e^{(-0.031t)} \quad (36)$$

The reference results were obtained through the simulation in Dymola (an overview of the Dymola model is given in Annex Fig. A). A comparison between the above functions and the simulation is provided in Fig. 8(a),

in which the results are close to each other, with a maximum 0.008K deviation, and it is caused by the selected significant figures.

Ramp signal

When the inlet parameters change with the ramp signal, the ramp signal's time duration is set to be 20s. Since the mass flowrate can only evolve with the step signal as the model's assumption, the next study is carried out in two conditions: inlet temperature ramp change (scenario 1), and simultaneous inlet temperature change together with mass flowrate step change (scenario 3). The analytical solutions based on the developed method are reached as follows.

Only inlet temperature change (scenario 1):

$$\begin{aligned} T_{c1,out}(t) &= 457 + 2858e^{(-0.049t)} - 448e^{(-0.060t)} - 54953e^{(-0.037t)} + 59100e^{(-0.036t)} - 6578e^{(-0.031t)} + 0.127t, 0 \le t \le 20s \\ T_{c1,out}(t) &= 438 + 104e^{(-0.049t)} - 15.8e^{(-0.060t)} - 807e^{(-0.037t)} + 784e^{(-0.036t)} - 58.2e^{(-0.031t)}, t > 20s \end{aligned} \quad (37)$$

Simultaneous change (scenario 3):

$$\begin{aligned} T_{c1,out}(t) &= 495 + 6704e^{(-0.049t)} - 981e^{(-0.060t)} - 13369e^{(-0.037t)} + 143034e^{(-0.036t)} - 15132e^{(-0.031t)} + 0.266t, 0 \le t \le 20s \\ T_{c1,out}(t) &= 455 + 81.6e^{(-0.049t)} - 7.82e^{(-0.060t)} - 635e^{(-0.037t)} + 623e^{(-0.036t)} - 67.7e^{(-0.031t)}, t > 20s \end{aligned} \quad (38)$$

The comparison between the analytical model and the simulation in Dymola is depicted in Fig. 8(b). The results are very close to each other, with a maximum error of about 0.02K, which can be regarded as the error caused by the selected significant figures. The corner of the outlet temperature function in Fig. 8(b) for both the inlet temperature change and the simultaneous change in the 20s can be noticed since the ramp signals stop there.

Without the pathway analysis and the presented technique of decomposition, it is possible to reach the Laplace function of the outlet temperature by applying directly the HE model on all the HEs which link from the inlets to the outlets. However, the obtained function is quite complex and a numerical method for Laplace transform inversion is required to get the function in the time domain. In practice, the common tools like Matlab or WolframAlpha usually fail to get the inverse Laplace transform, even for a smaller network compared to the one used in the example.

The results shown in this part confirm a correct implementation of the analytical model in Python. Before applying the model in a HEN design problem, the potential bias due to the assumptions made in the analytical model will be studied.

3.2 The potential error of the model

The analytical model is built with approximations to simplify the analysis, which will lead to bias compared with the real performance, and it is valuable to study the potential error. To approach the real result, the simulation platform Dymola together with the finite volume method was adopted, as shown in Fig. 9, in which each cell was built in Dymola and followed the same governing eqs. (1) ~ (3).

This work uses a typical case study to estimate the potential error. The case study is carried out toward a HE, where the parameters are given in Table 5, and the inlet temperature of cold and hot streams are assumed to follow the step signals, the heat capacity of the metal wall is set to be 2600 kJ/K.

1, 2, 4, 8, 16, and 32 different numbers of cells are selected to discretize the HE to approach the reference results gradually. The dynamic responses of H1 outlet temperature are depicted in Fig. 10. From the

observation, all these six curves evolve in the same trend. In terms of the temperature difference, 2 cells based model made substantial progress than 1 cell, and a step further with 4 cells based model. However, the progress from 8 cells is quite little, and the lines of 16 cells and 32 cells almost overlap.

Three indicators are proposed to interpret the difference, which are mean average error (MAE), mean average percent error (MAPE) and the response time. The response time describes the time duration required to reach stable status after changing operational conditions, and the stable status means all the curve are within 0.1% deviation compared with the value in infinite time. The calculation of MAE and MAPE depends on the response time, and are detailed in eqs. (39) and (40), in which 32 cells based results can be taken as reference.

$$MAE = \frac{\sum_{i}^{n} \left| y_i - y_i^o \right|}{n} \tag{39}$$

$$MAPE = \frac{\sum_{i}^{n} \left| y_i - y_i^o \right| / y_i}{n} * 100\% \tag{40}$$

where y_i is the current value, y_i^o is the reference value, and n stands for the total number of points within the duration of response time.

The error of MAE, MAPE and response time are provided in Table 6. Compared with the 32 cells based model, the MAE shows about 5 K error for the analytical HE dynamic model in this case study, and MAPE corresponds to about 1.18%. In the aspect of response time, it gets about 25.80% error, which can be acceptable when focus more in the relationship of various HENs rather than the absolute value, and it will be discussed in detail in the following application.

4. Application in a HEN design problem

The HEN design aims to balance the heat removing and demand between the hot streams and cold streams through optimized HEs, and reduce the consumption of utilities. Usually, the objective of the synthesis is to achieve the cost optimal design with a specific HEN structure. However, the dynamic performance of the optimized structure cannot be guaranteed, since it will be affected directly by the structure and the parameters. As discussed in Introduction part, some researchers have already realized that it is important to take the dynamic performance into consideration in the design stage to achieve fast response, otherwise it might take long time to achieve the operational transition and has significant impacts on the overall performance of the network.

Utilizing the above analytical model, an optimal cost design with desired dynamic performance can be reached. Since the model can only be applied in a complete HEN (the structure and all the parameters of HEs are known), it cannot be integrated into the simultaneous HEN synthesis models. The proposed model can be coupled with an optimization strategy such as the meta-heuristics based synthesis approach [28][29][30]. In which enormous structures will be generated and optimized, and they can carry out dynamic study with the above analytical model. Among the considerable methods, simulated annealing (SA) is one of the most common and efficient methods, and it was selected as the synthesis method in this work. The parameters of SA and synthesis models take [27] as reference, and each generated structure was optimized by Ipopt solver to find the optimal TAC and

the corresponding parameters of the network (flowrates, temperatures, heat exchanger areas …). The SA synthesis process is described in Fig. 11, it starts with an empty solution without any process HE (only utilities used) and a corresponding high cost structure. Then it will be perturbed to generate a new structure, and the optimized TAC will be compared with the actual solution. The structure will be updated when there is TAC progress. Even in the case of no progress in TAC, the structure still has a chance to be accepted by measuring the acceptance criteria. Each round, the analytical model will be applied to updated HEN to calculate the response time. Finally, the optimization process stops when reaching the maximum iteration steps, and the cost – response time trade-off results can be obtained.

Here, the analytical model is applied in a four stream case study, it is a multi-period synthesis problem also discussed by [31][32][33] with stream data shown in Table 7. The case problem is composed of two hot streams, two cold streams and supposed to work in three operational periods. The area cost is the investment cost of HE as function of heat transfer area, the annualizing cost transfers the investment into yearly cost. CHU and CCU describe the utility costs of cold stream and hot stream separately. Selecting different streams to measure the response time in different operational period change condition will likely lead to various results, and it depends largely on the specific industry process. Here, the response time in the case depicts the time duration required by all the hot streams changing from operational period 3 to period 1. The computer employed for the calculation is equipped with Intel Xeon (R) CPU 3.5GHz 32Gb. Carrying out the synthesis work, the trade-off results of cost and dynamic performance are obtained and illustrated in Fig. 12.

The results show that the response time of various designs can vary up to 10 times in spite of they get similar cost performance. With such large difference, the analytical model is believed to be able to identify the fast structures. It can be also observed that the response time can be improved with sacrificing only a bit of economic cost, such as in the region close to 200 k$/year.

Three representative HENs are selected as marked in Fig. 12 to take a deeper look into their structures and differences. The three selected structures are given in Fig. 13, HEN1 is the optimal TAC design that requires the longest response time (703s) among the three structures. It gets one more HEs than HEN2, has two stream splits, so that the structure is more complex as can be observed from the graph. There is no stream split happening in HEN2 which has the same number of utilities as with HEN1. HEN3 is free of process HE and only equipped with utilities; it gets the shortest response time among all the structures, but is the most expensive HEN.

The simulation tool was employed to check the response time relationship estimated by the analytical model. The simulation method has been described in the model validation part and the model of 16 cells is used to obtain the reference results. Applying 0.1% deviation (of final stable value in K) as the criteria to calculate the response time, the simulated response times of these three HENs are provided in Table 8. Even though the deviation of the response time obtained by the analytical model is evident compared to the simulated results, but the response time ranking defined by the analytical model is still correct. HEN1 requires a longer time than HEN2 to transfer from period 3 to period 1, and HEN3 is the fastest one. This confirms the effectiveness of the analytical model which can act as a pre-selection tool in the design stage to help designers select the fast

structures. It can also be noticed that the deviation of response time between the model and the simulation of HEN3 is larger than other structures. That might be because HEN3 gets no process HE, all the heat transfer relies on the utilities, the heat capacity flows of the streams in the utilities vary a lot and the model bias is magnified.

The analytical model allows to consider an additional dimension (dynamic performance) in the HEN design problem. The optimization part, alone, requires about 130s to finish, and the analytical calculation part demands about 17s. The analytical model calculation accounts for about 13% of the synthesis time, and the model works fluently during the calculation without any difficulty to converge.

5. Conclusions

In this paper, a decomposition-based strategy was proposed to obtain the HEN outlet temperature function analytically when there is an operational changeover. The method bases on the Laplace transform and a pathway analysis is used to obtain easily, without any difficulty of convergence, the function in the time domain. The analytical method can deal with any form of the inlet temperatures which can be expressed by a combination of step, ramp, and exponential signals. The potential bias of the analytic model has been illustrated through a simple HE case study by comparing with the reference result obtained by finite volume method.

As an example of application, the analytical model has been applied in a HEN synthesis problem to study the trade-off between the response time and the economic cost toward optimized structures. The results found that the dynamic performances of various designs differ considerably. Selecting three HENs with large difference in response time and economic cost, the relationship of the response time estimated by the analytical model still holds after validation with the simulation tools that approach to the real performance. The analytical model proposed in this work is an efficient and reliable tool to estimate the HEN dynamic performance in the design stage. However, it has also to be noticed that the model can only act as the pre-selection tool due to the simplifications of the dynamic model, which also requires validation through rigorous simulation results.

In further work, the model will be extended to consider not only counter-current and co-current heat exchangers, but also the cross flow configuration by using the F-factor. In addition, the heat capacity of the shell, of which the temperature approaches the temperature of one of the fluids rather than an average of the two fluids, will be included in the model. Finally, it will be necessary to develop a systematic method that quantifies the error of the model due to the assumption of the arithmetic mean temperature driving force.

Acknowledgement

The authors are very grateful for the grants from China Scholarship Council (CSC).

References

[1] M. Picon-Nunez, G.T. Polley, Determination of the steady state response of heat exchanger networks without simulation, Chem. Eng. Res. Des. 73 (1995) 941–952.

[2] L. Liu, Y. Bai, L. Zhang, S. Gu, J. Du, Synthesis of Flexible Heat Exchanger Networks Considering Gradually Accumulated Deposit and Cleaning Management, Ind. Eng. Chem. Res. 58 (2019) 12124–12136. https://doi.org/10.1021/acs.iecr.9b01672.

[3] S.S. Jogwar, M. Baldea, P. Daoutidis, Dynamics and Control of Energy Integrated Networks: A Multi - Time Scale Perspective, in: AIChE Annu. Meet., 2007.

[4] J. Fricker, C. Maatouk, A. Zoughaib, Simulating load variations of an integrated process operating with heat pump in order to improve design and control strategies, in: 26th Int. Conf. Effic. Cost, Optim. Simul. Environ. Impact Energy Syst., 2013.
[5] L. Payet, Remodelage de réseaux d'échangeurs de chaleur : collecte de données avancée, diagnostic énergétique et flexibilité., Ph.D. thesis. Institut national polytechnique de Toulouse, 2018.
[6] Q.Z. Yan, Y.H. Yang, Y.L. Huang, Cost-effective bypass design of highly controllable heat-exchanger networks, AIChE J. 47 (2001) 2253–2276. https://doi.org/10.1002/aic.690471012.
[7] M. Escobar, J.O. Trierweiler, Operational Controllability of Heat Exchanger Networks, IFAC, 2011. https://doi.org/10.3182/20100705-3-BE-2011.00017.
[8] L. Sun, X. Zha, X. Luo, Coordination between bypass control and economic optimization for heat exchanger network, Energy. 160 (2018) 318–329. https://doi.org/10.1016/j.energy.2018.07.021.
[9] G.Starace, M.Fiorentino, M.P.Longo, E.Carluccio, A hybrid method for the cross flow compact heat exchanger design, Appl. Therm. Eng. 111 (2017) 1129–1142.
[10] M. Fiorentino, G. Starace, The design of countercurrent evaporative condensers with the hybrid method, Appl. Therm. Eng. 130 (2018) 889–898. https://doi.org/10.1016/j.applthermaleng.2017.11.076.
[11] G.Starace, M.Fiorentino, B.Meleleo, C.Risolo, The hybrid method applied to the plate-finned tube evaporator geometry, Int. J. Refrig. 88 (2018) 67–77.
[12] S. Papastratos, A. Isambert, D. Depeyre, Computerized optimum design and dynamic simulation of heat exchanger networks, Comput. Chem. Eng. 17 (1993) S329–S334. https://doi.org/10.1016/0098-1354(93)80247-K.
[13] K.W. Mathisen, M. Morari, Dynamic models for heat exchangers and heat exchanger networks, Comput. Chem. Eng. 18 (1994) 459–463. https://doi.org/10.1016/0098-1354(94)80075-8.
[14] J. Chen, G. Cui, Y. Xiao, An analytical solution to the dynamic behavior of heat exchanger networks, Int. J. Heat Mass Transf. 126 (2018) 466–478. https://doi.org/10.1016/j.ijheatmasstransfer.2018.05.041.
[15] C. Boyaci, D. Uztork, U. Akman, Dynamics and optimal control of flexible heat exchanger networks, Comput. Chem. Engng. 20 (1996) 775–780.
[16] S. Hernández, L. Balcazar-Lopez, J.. Sanchez-Marquez, G. Gonzalez-Garcia, Controllability and operability analysis of heat exchanger networks including bypasses, Chem. Biochem. Eng. Q. 24 (2010) 23–28.
[17] M. Rathjens, T. Bohnenstädt, G. Fieg, O. Engel, Synthesis of heat exchanger networks taking into account cost and dynamic considerations, Procedia Eng. 157 (2016) 341–348. https://doi.org/10.1016/j.proeng.2016.08.375.
[18] D. Gvozdenac, Analytical solution of dynamic response of heat exchanger, Dr. Jovan Mitrovic (Ed.), InTech, 2012. https://doi.org/10.5772/35944.
[19] M. Lachi, N. El Wakil, J. Padet, The time constant of double pipe and one pass shell-and-tube heat exchangers in the case of varying fluid flow rates, Int. J. Heat Mass Transf. 40 (1997) 2067–2079. https://doi.org/10.1016/S0017-9310(96)00274-8.
[20] F.E. Romie, Response of counterflow heat exchangers to step changes of flow rates, J. Heat Transfer. 121 (1999) 746–748. https://doi.org/10.1115/1.2826046.
[21] W. Roetzel, Y. Xuan, Transient response of parallel and counterflow heat exchangers, Trans. ASME. 114 (1992) 510–512.
[22] J. Yin, M.K. Jensen, Analytic model for transient heat exchanger response, Int. J. Heat Mass Transf. 46 (2003) 3255–3264. https://doi.org/10.1016/S0017-9310(03)00118-2.
[23] W.C. Reynolds, T.A. Dolton, Use of integral methods in transient heat-transfer analysis, ASME. 58-A-248 (1959).
[24] Roetzel W., M.Li, X.Luo, Dynamic behaviour of heat exchangers, Adv. Comput. Methods Heat Transf. 20 (2002) 451–460.
[25] F.E. Romie, Transient response of the counterflow heat exchanger, J. Heat Transfer. 106 (1984) 620–626. https://doi.org/10.1115/1.3246725.
[26] S.A. GIREI, Optimal design and operation of heat exchanger network, Cranfield University, 2015.
[27] M.C. Aguitoni, L.V. Pavão, M. Antonio da Silva Sá Ravagnani, Heat exchanger network synthesis combining Simulated Annealing and Differential Evolution, Energy. 181 (2019) 654–664. https://doi.org/10.1016/j.energy.2019.05.211.
[28] R.I. Núñez-Serna, J.M. Zamora, NLP model and stochastic multi-start optimization approach for heat exchanger networks, Appl. Therm. Eng. 94 (2016) 458–471.
[29] Z. Bao, G. Cui, J. Chen, T. Sun, Y. Xiao, A novel random walk algorithm with compulsive evolution combined with an optimum-protection strategy for heat exchanger network synthesis, Energy. 152 (2018) 694–708. https://doi.org/10.1016/j.energy.2018.03.170.
[30] C.B. Miranda, C.B.B. Costa, J.A. Caballero, M.A.S.S. Ravagnani, Optimal synthesis of multiperiod heat exchanger networks: A sequential approach, Appl. Therm. Eng. 115 (2017) 1187–1202. https://doi.org/10.1016/j.applthermaleng.2016.10.003.

[31] D. Jiang, C.T. Chang, A new approach to generate flexible multiperiod heat exchanger network designs with timesharing mechanisms, Ind. Eng. Chem. Res. 52 (2013) 3794–3804. https://doi.org/10.1021/ie301075v.
[32] L. V. Pavão, C.B. Miranda, C.B.B. Costa, M.A.S.S. Ravagnani, Efficient multiperiod heat exchanger network synthesis using a meta-heuristic approach, Energy. 142 (2018) 356–372. https://doi.org/10.1016/j.energy.2017.09.147.
[33] C.B. Miranda, C.B.B. Costa, J.A. Caballero, M.A.S.S. Ravagnani, Optimal synthesis of multiperiod heat exchanger networks : A sequential approach, Appl. Therm. Eng. 115 (2016) 1187–1202. https://doi.org/10.1016/j.applthermaleng.2016.10.003.

Annex

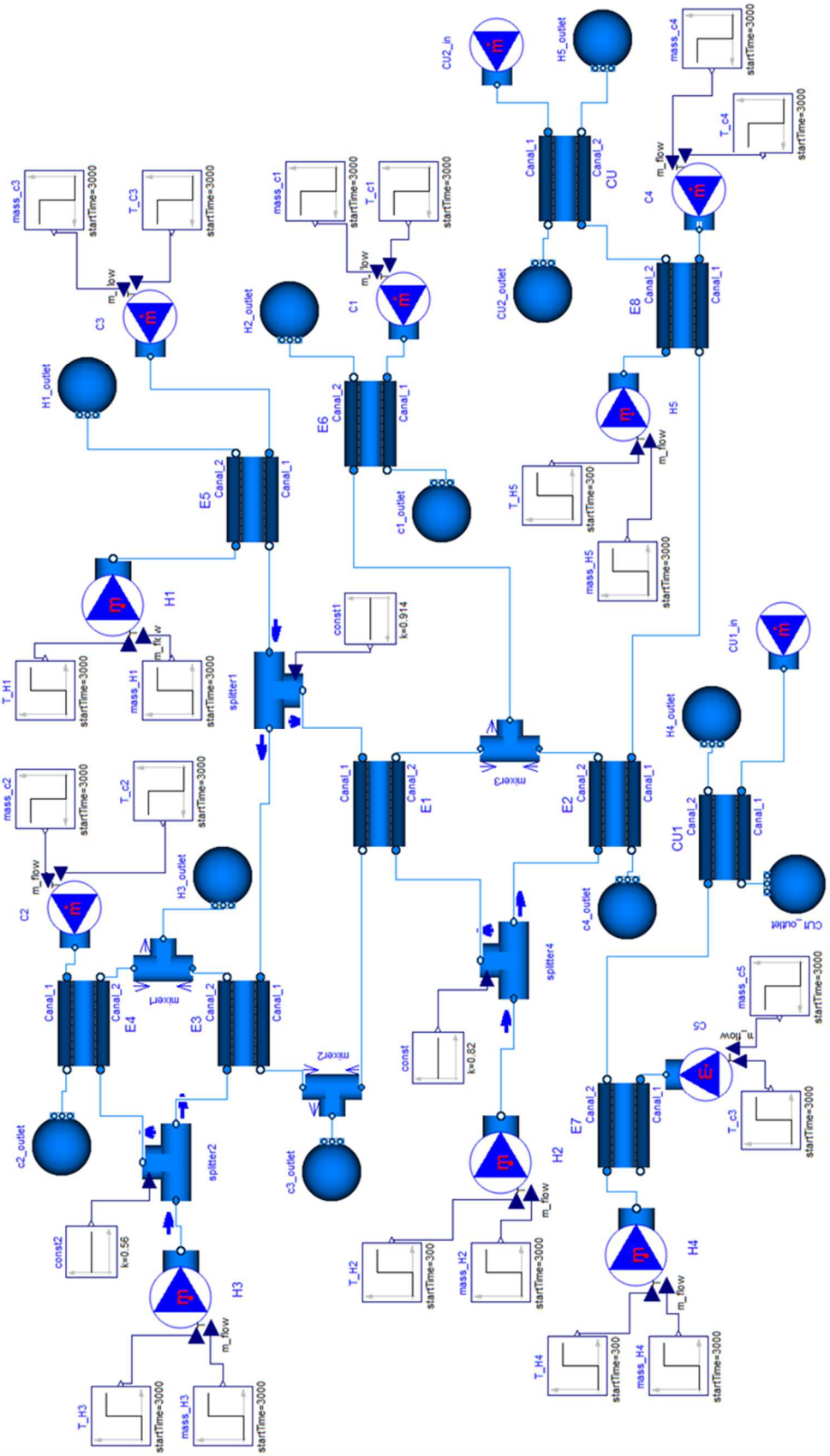

Fig. A1. Dymola interface to validate the analytic model toward example in Fig 7

Table A1. Pathway and corresponding transfer function of the HEs in series

Pathway	Sub-function
1	$T_{c1,1}(s) * g_{12}^{E3}(s) * f_{2}^{E1}(s) * g_{2}^{E2}(s) * g_{11}^{HU}(s)$
2	$T_{c1,1}(s) * g_{12}^{E3}(s) * f_{2}^{E1}(s) * g_{2}^{E2}(s) * g_{12}^{HU}(s)$
3	$T_{c1,1}(s) * g_{11}^{E3}(s) * f_{2}^{E1}(s) * g_{2}^{E2}(s) * g_{11}^{HU}(s)$
4	$T_{c1,1}(s) * g_{11}^{E3}(s) * f_{2}^{E1}(s) * g_{2}^{E2}(s) * g_{12}^{HU}(s)$
5	$T_{h1,1}(s) * g_{2}^{E3}(s) * f_{2}^{E1}(s) * g_{2}^{E2}(s) * g_{11}^{HU}(s)$
6	$T_{h1,1}(s) * g_{2}^{E3}(s) * f_{2}^{E1}(s) * g_{2}^{E2}(s) * g_{12}^{HU}(s)$
7	$T_{w}^{E3}(0) * g_{3}^{E3}(s) * f_{2}^{E1}(s) * g_{2}^{E2}(s) * g_{11}^{HU}(s)$
8	$T_{w}^{E3}(0) * g_{3}^{E3}(s) * f_{2}^{E1}(s) * g_{2}^{E2}(s) * g_{12}^{HU}(s)$
9	$T_{h2,1}(s) * \lambda_1 * g_{2}^{E2}(s) * g_{11}^{HU}(s)$
10	$T_{h2,1}(s) * \lambda_1 * g_{2}^{E2}(s) * g_{12}^{HU}(s)$
11	$T_{h2,1}(s) * (1-\lambda_1) * f_{12}^{E1}(s) * g_{2}^{E2}(s) * g_{11}^{HU}(s)$
12	$T_{h2,1}(s) * (1-\lambda_1) * f_{12}^{E1}(s) * g_{2}^{E2}(s) * g_{12}^{HU}(s)$
13	$T_{h2,1}(s) * (1-\lambda_1) * f_{11}^{E1}(s) * g_{2}^{E2}(s) * g_{11}^{HU}(s)$
14	$T_{h2,1}(s) * (1-\lambda_1) * f_{11}^{E1}(s) * g_{2}^{E2}(s) * g_{12}^{HU}(s)$
15	$T_{w}^{E1}(0) * f_{3}^{E1}(s) * g_{2}^{E2}(s) * g_{11}^{HU}(s)$
16	$T_{w}^{E1}(0) * f_{3}^{E1}(s) * g_{2}^{E2}(s) * g_{12}^{HU}(s)$
17	$T_{c2,1}(s) * g_{12}^{E2}(s) * g_{11}^{HU}(s)$
18	$T_{c2,1}(s) * g_{11}^{E2}(s) * g_{11}^{HU}(s)$
19	$T_{c2,1}(s) * g_{12}^{E2}(s) * g_{12}^{HU}(s)$
20	$T_{c2,1}(s) * g_{11}^{E2}(s) * g_{12}^{HU}(s)$
21	$T_{w}^{E2}(0) * g_{3}^{E2}(s) * g_{11}^{HU}(s)$
22	$T_{w}^{E2}(0) * g_{3}^{E2}(s) * g_{12}^{HU}(s)$
23	$T_{w}^{HU}(0) * g_{3}^{HU}(s)$
24	$T_{hu,in}(s) * g_{2}^{HU}(s)$

Table A2. Inverse Laplace results for all the pathways in the example of Fig 5

	Function in Laplace domain	Function in time domain
$G_1(s)$	$\frac{T_{c1,1}(0)}{s}\cdot b_{g_{12}}^{E3}\cdot\frac{b_{f_2}^{E1}}{s+a^{E1}}\cdot\frac{b_{g_2}^{E2}}{s+a^{E2}}\cdot\frac{b_{g_{11}}^{HU}}{s+a^{HU}}$	$\frac{T_{c1,1}(0)\cdot b_{g_{12}}^{E3}\cdot b_{f_2}^{E1}\cdot b_{g_2}^{E2}\cdot b_{g_{11}}^{HU}}{(a^{HU}-a^{E2})a^{E1}}\cdot\left(\begin{array}{l}\frac{1-e^{-a^{E2}t}}{a^{E2}}-\frac{1-e^{-a^{HU}t}}{a^{HU}}\\ -\frac{e^{-a^{E1}t}-e^{-a^{E2}t}}{a^{E2}-a^{E1}}+\frac{e^{-a^{E1}t}-e^{-a^{HU}t}}{a^{HU}-a^{E1}}\end{array}\right)$
$G_2(s)$	$\frac{T_{c1,1}(0)}{s}\cdot b_{g_{12}}^{E3}\cdot\frac{b_{f_2}^{E1}}{s+a^{E1}}\cdot\frac{b_{g_2}^{E2}}{s+a^{E2}}\cdot b_{g_{12}}^{HU}$	$\frac{T_{c1,1}(0)\cdot b_{g_{12}}^{E3}\cdot b_{f_2}^{E1}\cdot b_{g_2}^{E2}\cdot b_{g_{12}}^{HU}}{a^{E1}-a^{E12}}\cdot\left(\frac{1}{a^{E2}}(1-e^{-a^{E2}t})-\frac{1}{a^{E1}}(1-e^{-a^{E1}t})\right)$
$G_3(s)$	$\frac{T_{c1,1}(0)}{s}\cdot\frac{b_{g_{11}}^{E3}}{s+a^{E3}}\cdot\frac{b_{f_2}^{E1}}{s+a^{E1}}\cdot\frac{b_{g_2}^{E2}}{s+a^{E2}}\cdot\frac{b_{g_{11}}^{HU}}{s+a^{HU}}$	$\frac{T_{c1,1}(0)\cdot b_{g_{11}}^{E3}\cdot b_{f_2}^{E1}\cdot b_{g_2}^{E2}\cdot b_{g_{11}}^{HU}}{(a^{E1}-a^{E3})(a^{E2}-a^{HU})}\cdot\left(\begin{array}{l}\frac{1}{a^{HU}-a^{E3}}\left(\frac{1-e^{-a^{E3}t}}{a^{E3}}-\frac{1-e^{-a^{HU}t}}{a^{HU}}\right)\\ -\frac{1}{a^{E2}-a^{E3}}\left(\frac{1-e^{-a^{E3}t}}{a^{E3}}-\frac{1-e^{-a^{2}t}}{a^{E2}}\right)\\ -\frac{1}{a^{HU}-a^{E1}}\left(\frac{1-e^{-a^{E1}t}}{a^{E1}}-\frac{1-e^{-a^{HU}t}}{a^{HU}}\right)\\ +\frac{1}{a^{E2}-a^{E1}}\left(\frac{1-e^{-a^{E2}t}}{a^{E2}}-\frac{1-e^{-a^{E1}t}}{a^{E1}}\right)\end{array}\right)$
$G_4(s)$	$\frac{T_{c1,1}(0)}{s}\cdot\frac{b_{g_{11}}^{E3}}{s+a^{E3}}\cdot\frac{b_{f_2}^{E1}}{s+a^{E1}}\cdot\frac{b_{g_2}^{E2}}{s+a^{E2}}\cdot b_{g_{12}}^{HU}$	$\frac{T_{c1,1}(0)\cdot b_{g_{11}}^{E3}\cdot b_{f_2}^{E1}\cdot b_{g_2}^{E2}\cdot b_{g_{12}}^{HU}}{(a^{E3}-a^{E2})a^{E1}}\cdot\left(\begin{array}{l}\frac{1-e^{-a^{E2}t}}{a^{E2}}-\frac{1-e^{-a^{E3}t}}{a^{E3}}\\ -\frac{e^{-a^{E1}t}-e^{-a^{E2}t}}{a^{E2}-a^{E1}}+\frac{e^{-a^{E1}t}-e^{-a^{HU}t}}{a^{E3}-a^{E1}}\end{array}\right)$
$G_5(s)$	$\frac{T_{h1,1}(0)}{s}\cdot\frac{b_{g_2}^{E3}}{s+a^{E3}}\cdot\frac{b_{f_2}^{E1}}{s+a^{E1}}\cdot\frac{b_{g_2}^{E2}}{s+a^{E2}}\cdot\frac{b_{g_{11}}^{HU}}{s+a^{HU}}$	$\frac{T_{h1,1}(0)\cdot b_{g_2}^{E3}\cdot b_{f_2}^{E1}\cdot b_{g_2}^{E2}\cdot b_{g_{11}}^{HU}}{(a^{E1}-a^{E3})(a^{E2}-a^{HU})}\cdot\left(\begin{array}{l}\frac{1}{a^{HU}-a^{E3}}\left(\frac{1-e^{-a^{E3}t}}{a^{E3}}-\frac{1-e^{-a^{HU}t}}{a^{HU}}\right)\\ -\frac{1}{a^{E2}-a^{E3}}\left(\frac{1-e^{-a^{E3}t}}{a^{E3}}-\frac{1-e^{-a^{2}t}}{a^{E2}}\right)\\ -\frac{1}{a^{HU}-a^{E1}}\left(\frac{1-e^{-a^{E1}t}}{a^{E1}}-\frac{1-e^{-a^{HU}t}}{a^{HU}}\right)\\ +\frac{1}{a^{E2}-a^{E1}}\left(\frac{1-e^{-a^{E2}t}}{a^{E2}}-\frac{1-e^{-a^{E1}t}}{a^{E1}}\right)\end{array}\right)$
$G_6(s)$	$\frac{T_{h1,1}(0)}{s}\cdot\frac{b_{g_2}^{E3}}{s+a^{E3}}\cdot\frac{b_{f_2}^{E1}}{s+a^{E1}}\cdot\frac{b_{g_2}^{E2}}{s+a^{E2}}\cdot b_{g_{12}}^{HU}$	$\frac{T_{h1,1}(0)\cdot b_{g_2}^{E3}\cdot b_{f_2}^{E1}\cdot b_{g_2}^{E2}\cdot b_{g_{12}}^{HU}}{(a^{E3}-a^{E2})a^{E1}}\cdot\left(\begin{array}{l}\frac{1-e^{-a^{E2}t}}{a^{E2}}-\frac{1-e^{-a^{E3}t}}{a^{E3}}-\\ \frac{e^{-a^{E1}t}-e^{-a^{E2}t}}{a^{E2}-a^{E1}}+\frac{e^{-a^{E1}t}-e^{-a^{HU}t}}{a^{E3}-a^{E1}}\end{array}\right)$
$G_7(s)$	$T_w^{E3}(0)\cdot\frac{b_{g_3}^{E3}}{s+a^{E3}}\cdot\frac{b_{f_2}^{E1}}{s+a^{E1}}\cdot\frac{b_{g_2}^{E2}}{s+a^{E2}}\cdot\frac{b_{g_{11}}^{HU}}{s+a^{HU}}$	$\frac{T_w^{E3}(0)\cdot b_{g_3}^{E3}\cdot b_{f_2}^{E1}\cdot b_{g_2}^{E2}\cdot b_{g_{11}}^{HU}}{(a^{E1}-a^{E3})(a^{E2}-a^{HU})}\cdot\left(\begin{array}{l}\frac{e^{-a^{E3}t}-e^{-a^{HU}t}}{a^{HU}-a^{E3}}-\frac{e^{-a^{E2}t}-e^{-a^{E3}t}}{a^{E2}-a^{E3}}\\ -\frac{e^{-a^{HU}t}-e^{-a^{E1}t}}{a^{HU}-a^{E1}}+\frac{e^{-a^{E2}t}-e^{-a^{E1}t}}{a^{E2}-a^{E1}}\end{array}\right)$
$G_8(s)$	$T_w^{E3}(0)\cdot\frac{b_{g_3}^{E3}}{s+a^{E3}}\cdot\frac{b_{f_2}^{E1}}{s+a^{E1}}\cdot\frac{b_{g_2}^{E2}}{s+a^{E2}}\cdot b_{g_{12}}^{HU}$	$\frac{T_w^{E3}(0)\cdot b_{g_{12}}^{HU}}{a^{E1}-a^{E2}}\cdot\left(\begin{array}{l}\frac{1}{a^{E2}-a^{E3}}(e^{-a^{E3}t}-e^{-a^{E2}t})\\ -\frac{1}{a^{E1}-a^{E3}}(e^{-a^{E3}t}-e^{-a^{E1}t})\end{array}\right)$
$G_9(s)$	$\frac{T_{h2,1}(0)\cdot\lambda_1}{s}\cdot\frac{b_{g_2}^{E2}}{s+a^{E2}}\cdot\frac{b_{g_{11}}^{HU}}{s+a^{HU}}$	$\frac{T_{h2,1}(0)\cdot\lambda_1\cdot b_{g_2}^{E2}\cdot b_{g_{11}}^{HU}}{a^{HU}-a^{E2}}\cdot\left(\frac{1}{a^{E2}}(1-e^{-a^{E2}t})-\frac{1}{a^{HU}}(1-e^{-a^{HU}t})\right)$
$G_{10}(s)$	$\frac{T_{h2,1}(0)\cdot\lambda_1}{s}\cdot\frac{b_{g_2}^{E2}}{s+a^{E2}}\cdot b_{g_{12}}^{HU}$	$T_{h2,1}(0)\cdot\lambda_1\cdot\frac{b_{g_2}^{E2}\cdot b_{g_{12}}^{HU}}{a^{E2}}\cdot(1-e^{-a^{E2}t})$

$G_{11}(s)$	$\frac{T_{h2,1}(0)\cdot(1-\lambda_1)}{s}\cdot b_{f_{12}}^{E1}\cdot\frac{b_{g_2}^{E2}}{s+a^{E2}}\cdot\frac{b_{g_{11}}^{HU}}{s+a^{HU}}$	$\frac{T_{h2,1}(0)\cdot(1-\lambda_1)\cdot b_{f_{12}}^{E1}\cdot b_{g_2}^{E2}\cdot b_{g_{11}}^{HU}}{a^{HU}-a^{E2}}\cdot\left(\frac{1}{a^{E2}}(1-e^{-a^{E2}t})-\frac{1}{a^{HU}}(1-e^{-a^{HU}t})\right)$
$G_{12}(s)$	$\frac{T_{h2,1}(0)\cdot(1-\lambda_1)}{s}\cdot b_{f_{12}}^{E1}\cdot\frac{b_{g_2}^{E2}}{s+a^{E2}}\cdot b_{g_{12}}^{HU}$	$\frac{T_{h2,1}(0)\cdot(1-\lambda_1)\cdot b_{f_{12}}^{E1}\cdot b_{g_2}^{E2}\cdot b_{g_{12}}^{HU}}{a^{E2}}(1-e^{-a^{E2}t})$
$G_{13}(s)$	$\frac{T_{h2,1}(0)\cdot(1-\lambda_1)}{s}\cdot\frac{b_{f_{11}}^{E1}}{s+a^{E1}}\cdot\frac{b_{g_2}^{E2}}{s+a^{E2}}\cdot\frac{b_{g_{11}}^{HU}}{s+a^{HU}}$	$\frac{T_{h2,1}(0)\cdot(1-\lambda_1)\cdot b_{f_{11}}^{E1}\cdot b_{g_2}^{E2}\cdot b_{g_{11}}^{HU}}{(a^{HU}-a^{E2})a^{E1}}\cdot\left(\frac{1-e^{-a^{E2}t}}{a^{E2}}-\frac{1-e^{-a^{HU}t}}{a^{HU}}-\frac{e^{-a^{E1}t}-e^{-a^{E2}t}}{a^{E2}-a^{E1}}+\frac{e^{-a^{E1}t}-e^{-a^{HU}t}}{a^{HU}-a^{E1}}\right)$
$G_{14}(s)$	$\frac{T_{h2,1}(0)\cdot(1-\lambda_1)}{s}\cdot\frac{b_{f_{11}}^{E1}}{s+a^{E1}}\cdot\frac{b_{g_2}^{E2}}{s+a^{E2}}\cdot b_{g_{12}}^{HU}$	$\frac{T_{h2,1}(0)\cdot(1-\lambda_1)\cdot b_{f_{11}}^{E1}\cdot b_{g_2}^{E2}\cdot b_{g_{12}}^{HU}}{a^{E2}-a^{E1}}\cdot\left(\frac{1}{a^{E1}}(1-e^{-a^{E1}t})-\frac{1}{a^{E2}}(1-e^{-a^{E2}t})\right)$
$G_{15}(s)$	$T_w^{E1}(0)\cdot\frac{b_{f_3}^{E1}}{s+a^{E1}}\cdot b_{g_2}^{E2}\cdot\frac{b_{g_{11}}^{HU}}{s+a^{HU}}$	$T_w^{E1}(0)\cdot b_{f_3}^{E1}\cdot b_{g_2}^{E2}\cdot b_{g_{11}}^{HU}\cdot\frac{e^{a^{-E1}t}-e^{-a^{HU}t}}{a^{HU}-a^{E1}}$
$G_{16}(s)$	$T_w^{E1}(0)\cdot\frac{b_{f_3}^{E1}}{s+a^{E1}}\cdot b_{g_2}^{E2}\cdot b_{g_{12}}^{HU}$	$T_w^{E1}(0)\cdot b_{f_3}^{E1}\cdot b_{g_2}^{E2}\cdot b_{g_{12}}^{HU}\cdot e^{-a^{E1}t}$
$G_{17}(s)$	$\frac{T_{c2,1}(0)}{s}\cdot b_{g_{12}}^{E2}\cdot\frac{b_{g_{11}}^{HU}}{s+a^{HU}}$	$\frac{T_{c2,1}(0)\cdot b_{g_{12}}^{E2}\cdot b_{g_{11}}^{HU}}{a^{HU}}\left(1-e^{-a^{HU}t}\right)$
$G_{18}(s)$	$\frac{T_{c2,1}(0)}{s}\cdot\frac{b_{g_{11}}^{E2}}{s+a^{E2}}\cdot\frac{b_{g_{11}}^{HU}}{s+a^{HU}}$	$\frac{T_{c2,1}(0)\cdot b_{g_{11}}^{E2}\cdot b_{g_{11}}^{HU}}{a^{HU}-a^{E2}}\cdot(\frac{1-e^{-a^{E2}t}}{a^{E2}}-\frac{1-e^{-a^{HU}t}}{a^{HU}})$
$G_{19}(s)$	$\frac{T_{c2,1}(0)}{s}\cdot b_{g_{12}}^{E2}\cdot b_{g_{12}}^{HU}$	$T_{c2,1}(0)\cdot b_{g_{12}}^{E2}\cdot b_{g_{12}}^{HU}$
$G_{20}(s)$	$\frac{T_{c2,1}(0)}{s}\cdot\frac{b_{g_{11}}^{E2}}{s+a^{E2}}\cdot b_{g_{12}}^{HU}$	$\frac{T_{c2,1}(0)\cdot b_{g_{11}}^{E2}\cdot b_{g_{12}}^{HU}}{a^{E2}}\cdot(1-e^{-a^{E2}t})$
$G_{21}(s)$	$T_w^{E2}(0)\cdot\frac{b_{g_3}^{E2}}{s+a^{E2}}\cdot\frac{b_{g_{11}}^{HU}}{s+a^{HU}}$	$\frac{T_w^{E2}(0)\cdot b_{g_3}^{E2}\cdot b_{g_{11}}^{HU}}{a^{HU}-a^{E2}}\cdot(e^{-a^{E2}t}-e^{-a^{HU}t})$
$G_{22}(s)$	$T_w^{E2}(0)\cdot\frac{b_{g_3}^{E2}}{s+a^{E2}}\cdot b_{g_{12}}^{HU}$	$T_w^{E2}(0)\cdot b_{g_3}^{E2}\cdot b_{g_{12}}^{HU}\cdot e^{-a^{E2}t}$
$G_{23}(s)$	$T_w^{HU}(0)\cdot\frac{b_{g_3}^{HU}}{s+a^{HU}}$	$T_w^{HU}(0)\cdot b_{g_3}^{HU}\cdot e^{-a^{HU}t}$
$G_{24}(s)$	$\frac{T_{hu,in}(0)}{s}\cdot\frac{b_{g_2}^{HU}}{s+a^{HU}}$	$\frac{T_{hu,in}(0)\cdot b_{g_2}^{HU}}{a^{HU}}\left(1-e^{-a^{HU}t}\right)$

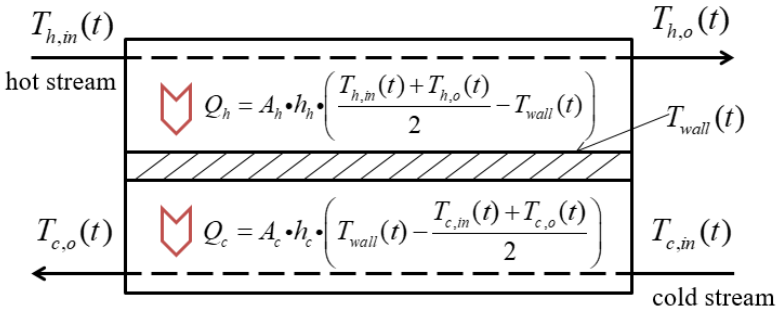

Fig 1. Simplified HE dynamic model

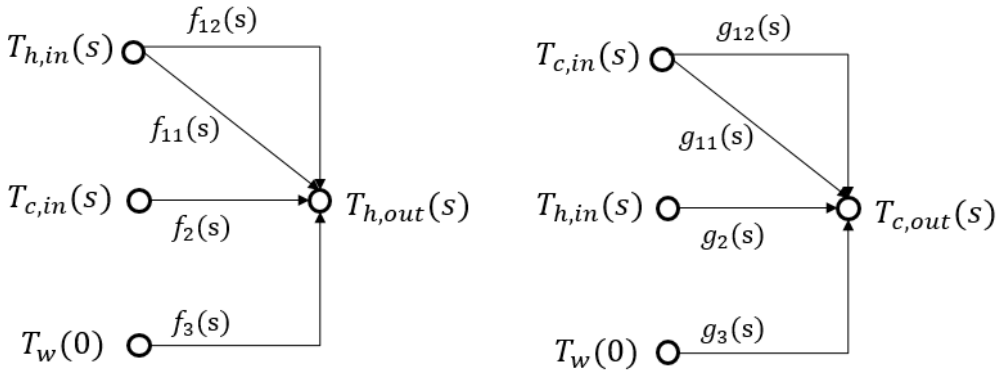

Fig 2. HE outlet temperature decomposition: pathway representation

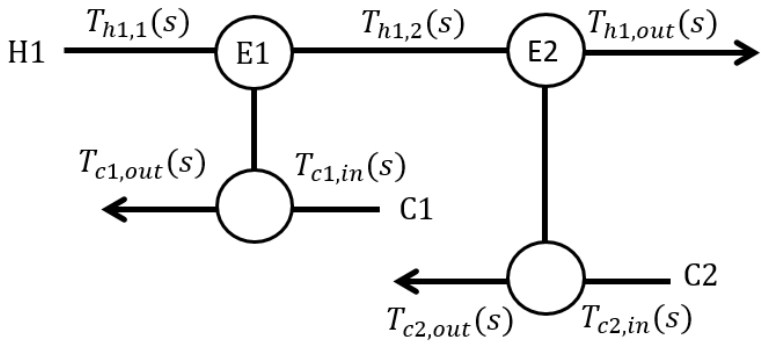

Fig 3. Example of HEs in-series

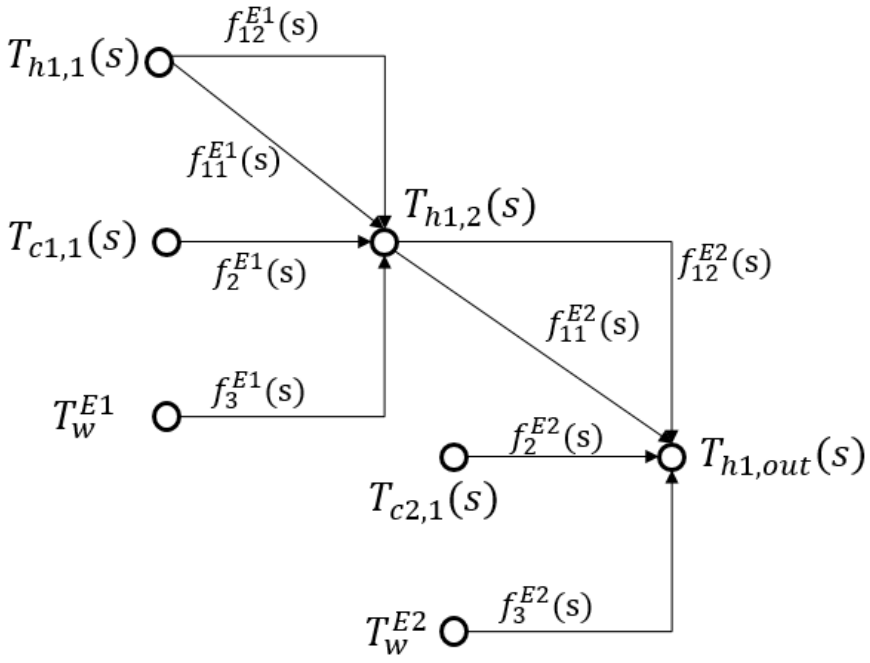

Fig 4. Pathway analysis of the HEs in series (example in Fig. 3)

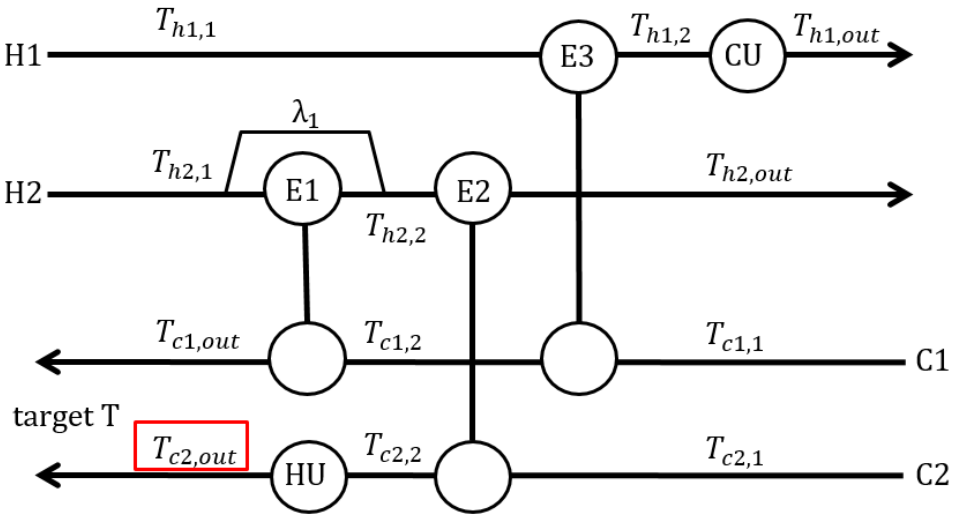

Fig 5. Example of HEN using HEs in-series and split

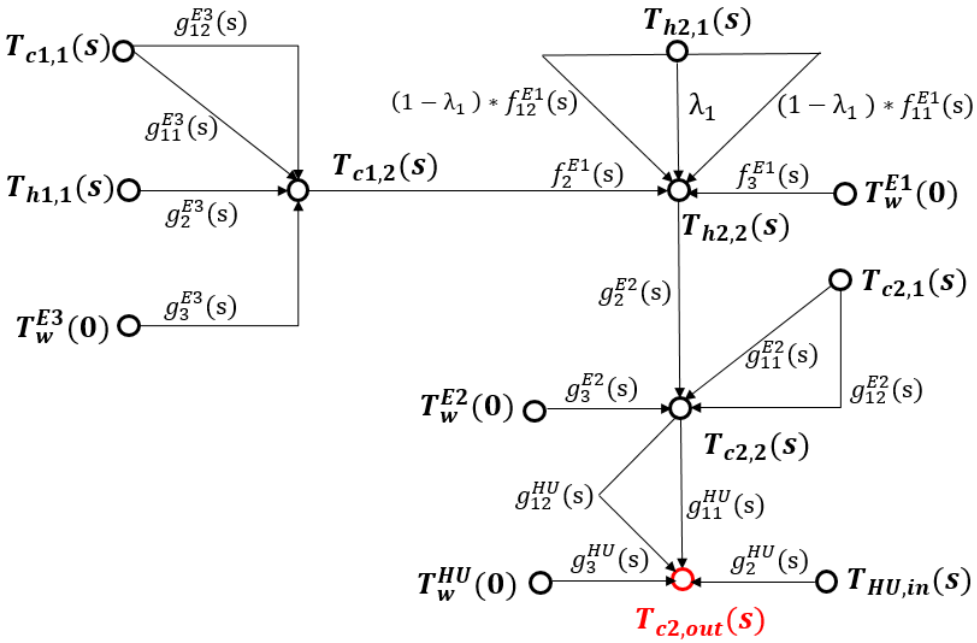

Fig 6. Pathway analysis toward the case example

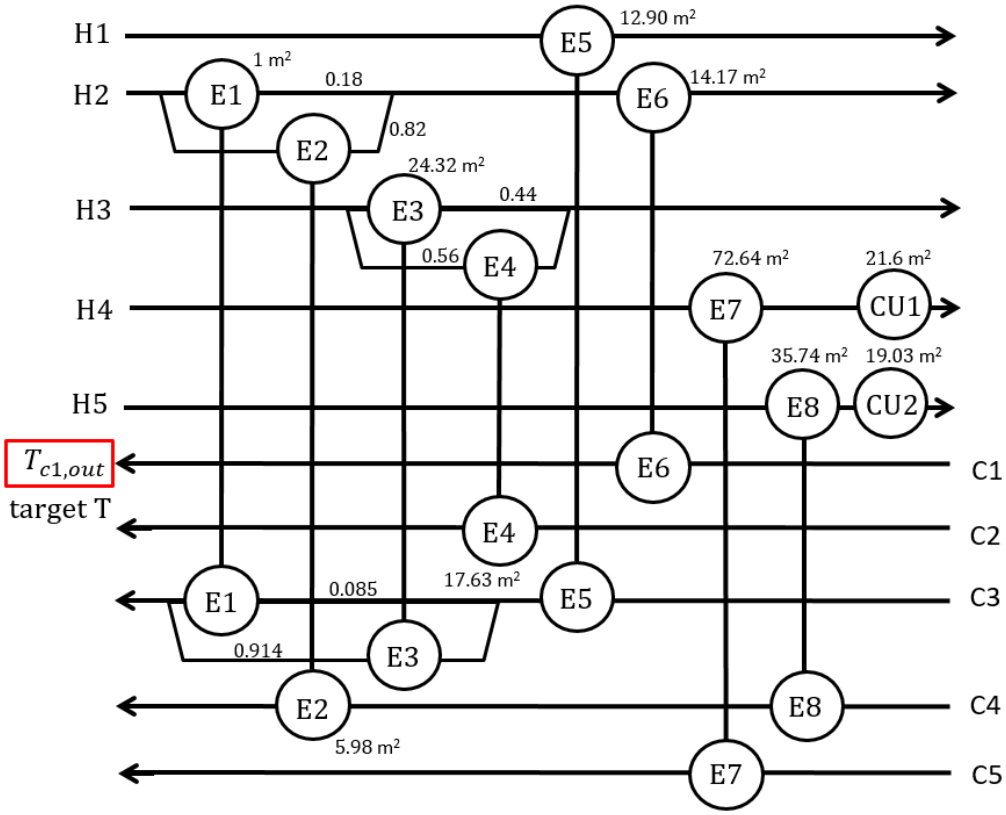

Fig 7. HEN example to validate the improved HEN dynamic model

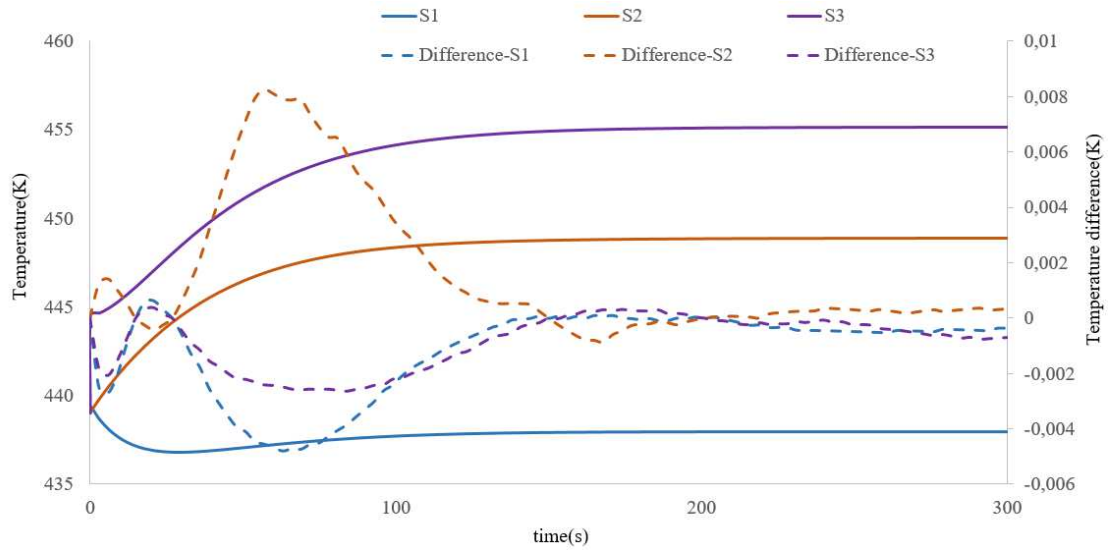

(a)

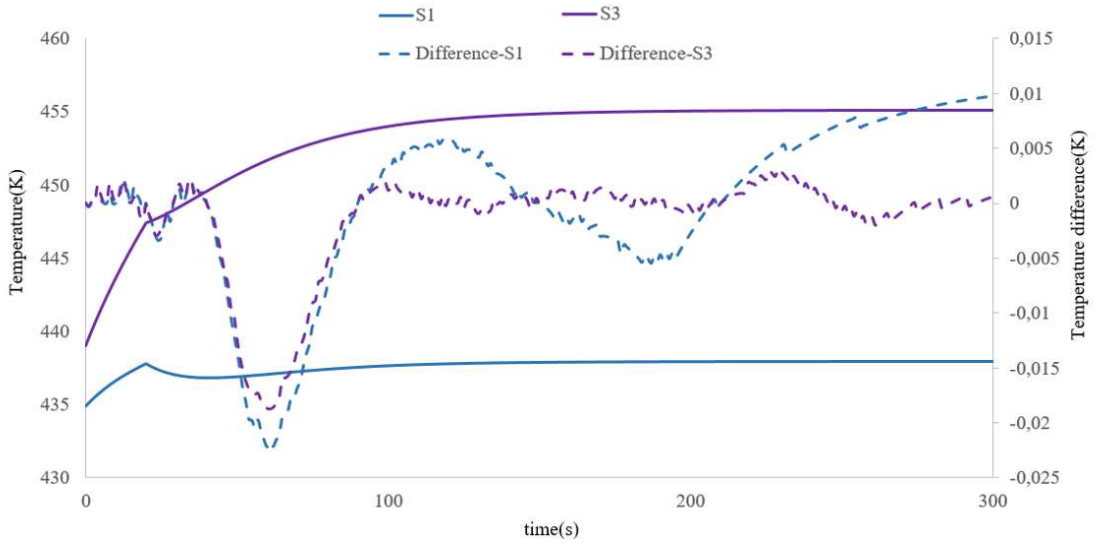

(b)

Fig 8. Comparison between the analytical model and simulation in Dymola: inlet temperatures follow step signals (a); ramp signal (b); (legend S – Scenario)

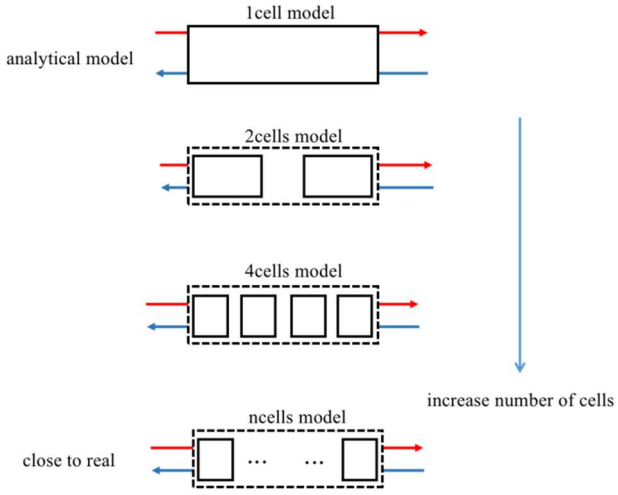

Fig 9. Illustration of the finite volume method to approach real performance of the HE in Dymola

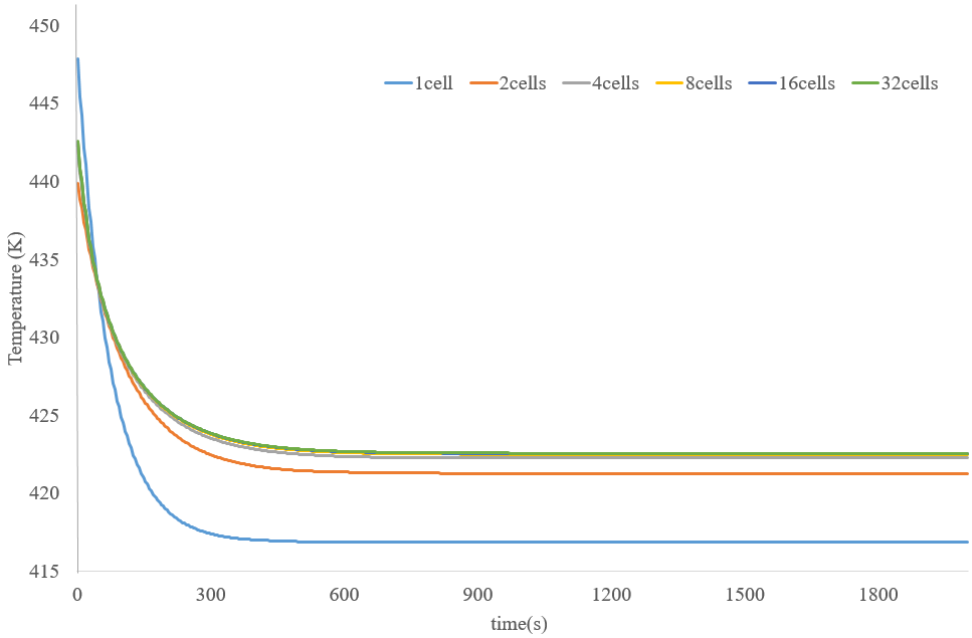

Fig 10. Dynamic response of hot outlet temperature according to different numbers of cells

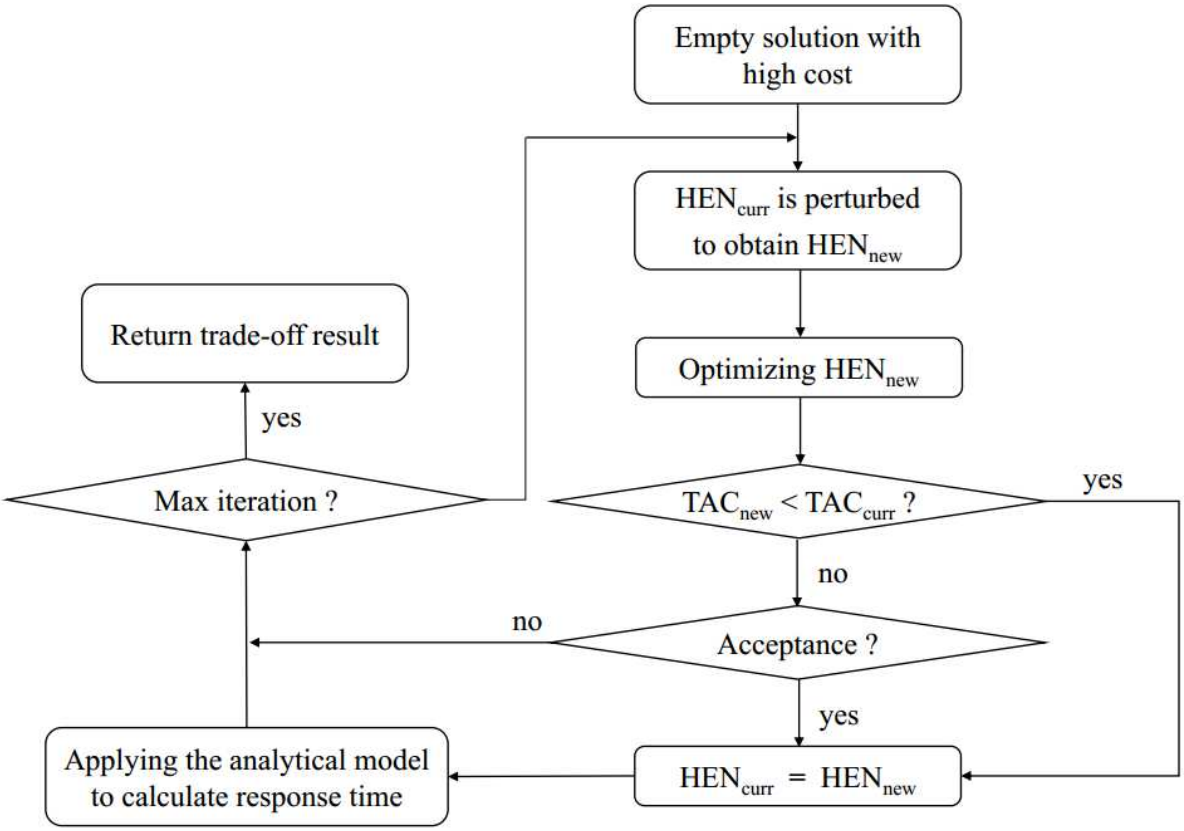

Fig 11. SA to carry out the synthesis work

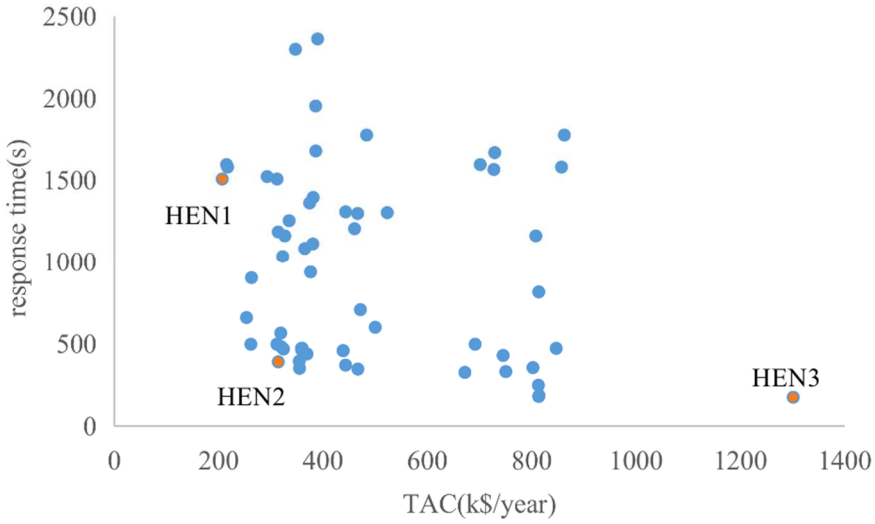

Fig 12. TAC- response time trade-off result

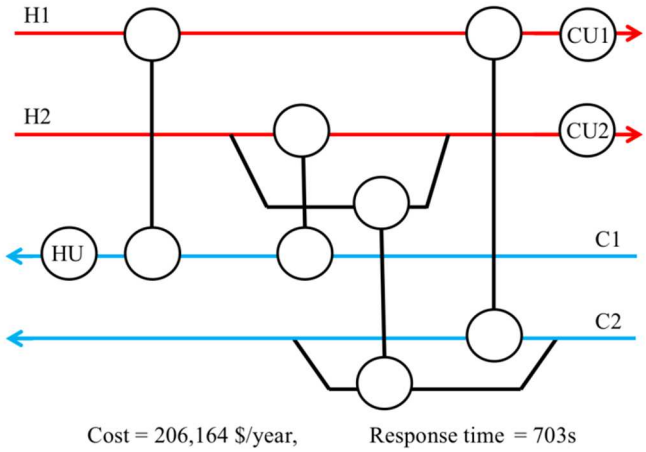

(a) HEN1 (optimal TAC)

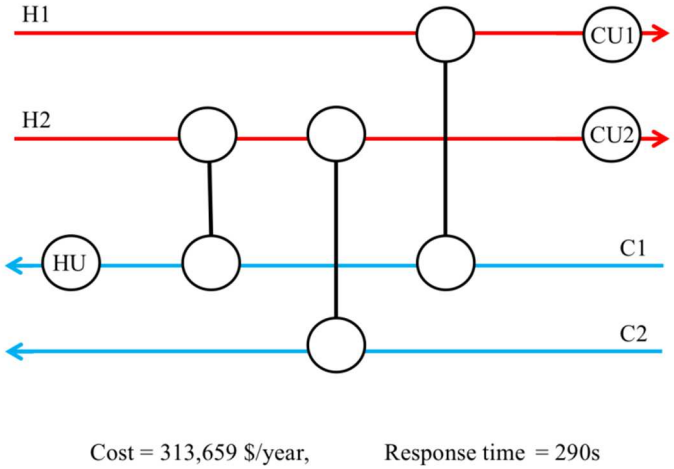

(b) HEN2

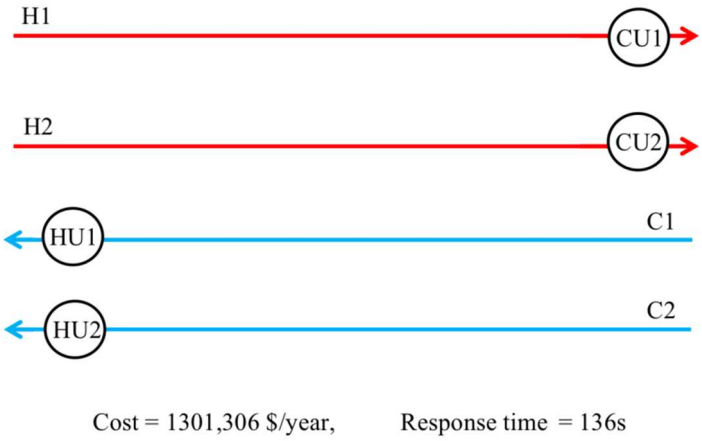

(c) HEN3

Fig 13. HEN designs in the pseudo Pareto-front of the TAC-response time trade-off results (see Fig. 12)

Table 1. Comparison of HEN dynamic model types

	Numerical simulation	Analytical
Pros	Complexity can be controlled by choosing the discretized cells number.	Fast calculation without convergence problem
Cons	Convergence difficulty, initial value setting	Complex expression

Table 2. Summary of HE analytical models

	Method	Temperature distribution	Simultaneous changes	Minor or significant change	Parameter calibration
Roetzel and Xuan[21]	First order transfer function	Yes	Yes	Minor	None
Lachi et al.[19]	Empirical exponential expression	No	No	Both	Experimental /simulation
Roetzel et al.[24]	Laplace Transform	No	Yes	Both	None
Yin and Jensen[22]	Integral	Yes	No	Both	None

Table 3. Pathway and corresponding function of the HEs in series (example in Fig.4)

Pathway	Function
1	$T_{h1,1}(s) * f_{12}^{E1}(s) * f_{12}^{E2}(s)$
2	$T_{h1,1}(s) * f_{11}^{E1}(s) * f_{12}^{E2}(s)$
3	$T_{c1,1}(s) * f_{2}^{E1}(s) * f_{12}^{E2}(s)$
4	$T_{w}^{E1}(s) * f_{2}^{E1}(s) * f_{12}^{E2}(s)$
5	$T_{h1,1}(s) * f_{12}^{E1}(s) * f_{11}^{E2}(s)$
6	$T_{h1,1}(s) * f_{11}^{E1}(s) * f_{11}^{E2}(s)$
7	$T_{c1,1}(s) * f_{2}^{E1}(s) * f_{11}^{E2}(s)$
8	$T_{w}^{E1}(s) * f_{3}^{E1}(s) * f_{11}^{E2}(s)$
9	$T_{c2,1}(s) * f_{2}^{E2}(s)$
10	$T_{w}^{E2}(s) * f_{3}^{E2}(s)$

Table 4. Parameters for the HEN example in Fig 7

Stream	T_{in}(K)	T_{out}(K)	CP(kW/K)	h (kW/m^2•K)
H1	433.15	366.15	8.79	1.704
H2	522.15	411.15	10.55	1.704
H3	544.15	422.15	12.56	1.704
H4	500.15	339.15	14.77	1.704
H5	472.15	339.15	17.73	1.704
C1	333.15	433.15	7.62	1.704
C2	389.15	495.15	6.08	1.704
C3	311.15	494.15	8.44	1.704
C4	355.15	450.15	17.28	1.704
C5	366.15	478.15	13.9	1.704
HU	509.15	509.15	-	3.408
CU	311.15	355.15	-	3.408

Table 5. Case study: HE parameters

	Inlet temperature (K)	Heat capacity flow (kW/K)	Heat transfer coefficient (kW/m^2•K)
Hot stream	650 to 630	10	1
Cold stream	410 to 390	15	1

Table 6. Dynamic performances of different models

	MAE (K)	MAPE	Response time (s)
Analytical model	4.729	1.11%	325
2 cells	1.365	0.32%	410
4 cells	0.248	0.06%	435
8 cells	0.058	0.01%	438
16 cells	0.013	0.00%	438
32 cells	-	-	438

Table 7. Stream data for the HEN design problem

	T_in (K)			T_out (K)			$\dot{m}cp$ (kW/K)			h (kW/m^2 K)		
	P1	P2	P3	P1	P2	P3	P1	P2	P3	P1	P2	P3
H1	650	630	645	370	380	350	10	10.2	10	1	1.03	1.01
H2	590	570	600	370	340	350	20	20.5	20.3	1	1.04	1.04
C1	410	390	420	640	630	660	15	15	14.3	1	1.02	1.05
C2	350	340	320	500	520	540	13	13.5	13	1	1.05	1.03

Area costs = $4333A^{0.6}$ $

Annualizing factor = 0.1/yr

CHU (680-680 K) = 150.163$/(kW•yr); hhu = 5 kW/(m^2•K)

CCU (300-320 K) = 53.064$/(kW•yr); hcu = 1 kW/(m^2•K)

Table 8. Response time results

HEN	response time (simulation)	response time (model)
HEN1	688s	703s
HEN2	358s	290s
HEN3	61s	136s